A sub-grid structure enhanced discontinuous Galerkin method for multiscale diffusion and convection-diffusion problems

Eric T. Chung* and Wing Tat Leung

Department of Mathematics, The Chinese University of Hong Kong, Hong Kong.

Abstract. In this paper, we present an efficient computational methodology for diffusion and convection-diffusion problems in highly heterogeneous media as well as convection-dominated diffusion problem. It is well known that the numerical computation for these problems requires a significant amount of computer memory and time. Nevertheless, the solutions to these problems typically contain a coarse component, which is usually the quantity of interest and can be represented with a small number of degrees of freedom. There are many methods that aim at the computation of the coarse component without resolving the full details of the solution. Our proposed method falls into the framework of interior penalty discontinuous Galerkin method, which is proved to be an effective and accurate class of methods for numerical solutions of partial differential equations. A distinctive feature of our method is that the solution space contains two components, namely a coarse space that gives a polynomial approximation to the coarse component in the traditional way and a multiscale space which contains sub-grid structures of the solution and is essential to the computation of the coarse component. In addition, stability of the method is proved. The numerical results indicate that the method can accurately capture the coarse behavior of the solution for problems in highly heterogeneous media as well as boundary and internal layers for convection-dominated problems.

Key words: multiscale problem, sub-grid capturing, multiscale basis function, boundary layer, internal layer

1 Introduction

Let $\Omega \subset \mathbb{R}^2$ be a domain in the two-dimensional space. We consider the following static convection-diffusion problem

$$\begin{aligned} \mathcal{L}(u) \equiv \nabla \cdot (\vec{b}u - a\nabla u) = f \quad &\text{in} \quad \Omega, \\ u = g \quad &\text{on} \quad \partial\Omega, \end{aligned} \tag{1.1}$$

*Corresponding author. *Email address:* tschung@math.cuhk.edu.hk

where $\vec{b}$ is a given divergence-free vector field, f and g are given source and boundary functions. We also consider the corresponding time-dependent problem

$$\begin{aligned} \frac{\partial u}{\partial t} + \mathcal{L}(u) &= f \quad \text{in} \quad (0,T)\times\Omega, \\ u &= g \quad \text{on} \quad (0,T)\times\partial\Omega, \\ u(0,x) &= u_0 \quad \text{in} \quad \Omega. \end{aligned} \tag{1.2}$$

In (1.1) and (1.2), we assume the ellipticity condition that $c_1 \geq a(x) \geq c_0 > 0$ for all $x \in \Omega$ and for some constants c_0 and c_1. Our aim in this work is the numerical approximation of (1.1) and (1.2) in the case when a and $\vec{b}$ are highly oscillatory or in the case when a is very small in some region that gives a convection-dominated diffusion problem. It is well-known that the solutions to these problems contain multiple scales, and the numerical computations require a very fine grid. Thus, a significant amount of computer memory and time are needed, and with the superior computing power nowadays, the computation of the solutions to these problems is still very challenging and sometimes even impossible. Nevertheless, the solutions to these problems typically contain a coarse component, which is usually the quantity of interest and can be represented by a small number of degrees of freedom. There are in literature many methods that aim at solving these problems on a coarse grid with great success. For example, see [5,6,12–15,17,20] for multiscale diffusion and wave problems and [16,21] for multiscale convection-diffusion problems.

The discontinuous Galerkin (DG) method is proved to be an effective and accurate class of tools for the numerical solutions of partial differential equations [1, 2, 4, 7–11]. The main idea is to use polynomial approximation on each cell without enforcing any continuity along cell interfaces. The success of these methods is achieved by using some sophisicated techniques to control the jumps. Due to the high efficiency and flexibility of DG methods, there are some advancement in using DG methods for the numerical approximation of problems with multiple scales. To the best of our knowledge, there are two existing classes of methods in literature. First of all, the discontinuous enrichment method has been proposed in [19] by Kalashnikova, Farhat and Tezaur. In this work, the solution space is discontinuous and contains two components, which is a polynomial space and a space spanned by the solution of local cell problem. One significant assumption is that the solutions of the local cell problems can be solved analytically. For problems with inhomogeneous media, the technique of frozen coefficient is applied. The formulation of the discrete problem is based on a DG framework, but the continuity is enforced by the method of Lagrange multiplier. The second class of method is the multiscale discontinuous Galerkin method proposed in [23] by Wang, Guzman and Shu. In this work, the interior penalty discontinuous Galerkin (IPDG) framework is used. Instead of using polynomials, the solution space is spanned by basis functions that are solutions of the given partial differential equation on each cell. To find these basis functions, the given partial differential equation imposed with suitable source functions is solved ana-

lytically on each coarse grid. Moreover, convergence of the method is proved for a class of material coefficients that allow the local cell problem to be solved analytically.

In this paper, we propose and study a novel methodology based on the framework of IPDG. The key element of our new method is the choice of local approximation space. Our local space is the direct sum of two components. The first component is the classical polynomial space without inter-element continuity. The second component is spanned by a set of basis functions that are the solutions of local cell problems arising from the given partial differential equation. In a sense, our method can be seen as the classical IPDG method with the finite element space enhanced by these basis functions. Even though our method shares some properties of the methods in [19, 23], there is a significant difference and improvement. For the local problem defined on a coarse grid block, we do not assume that there is any structure in the medium which implies that analytical solution cannot be found. It is then necessary to impose an artificial boundary condition on the cell boundary in order to obtain the solution. Ideally, we should impose the exact solution of the given problem as the boundary condition. However, since we do not know the exact solution, we can only impose an approximate boundary condition which provide an approximation to the correct behavior of the exact solution along cell boundaries. Among many choices of artificial boundary conditions, the uniform flux condition is a good choice, which is also successfully used for finding local basis functions for a multiscale flow problem in [18]. Therefore, we will numerically solve our local cell problem by imposing a Neumann boundary condition. In particular, we assume that the basis functions have unit flux on part of the cell boundary and zero flux on the rest of the boundary. These basis functions allow us to obtain an accurate approximation of the correct coarse scale behavior of the true solution, which is represented by the polynomial component of our solution space. Thus, our method has the advantage and potential to handle problems with very complex media.

The paper is organized as follows. In Section 2, we will present a detail description of our new sub-grid structure enhanced IPDG method and its stability analysis. The method is then discussed numerically in Section 3. Plenty of numerical simulation results are given to validate the effectiveness of our method. Finally a conclusion will be given.

2 The sub-grid structure enhanced IPDG method

2.1 Method description

We will first highlight the philosophy of our proposed approach. Our new sub-grid structure enhanced IPDG method is based on the classical framework of interior penalty discontinuous Galerkin method [22]. The main ingredient of the method is the choice of local approximation space. Our solution space is a direct sum of two parts. The first part is the classical piecewise polynomial space. The second part is spanned by a set of piecewise smooth basis functions, which are the solutions of local cell problems, similar to the multiscale finite element idea, see for example [13,17]. We emphasize that since we

do not assume any structure on the media, the local problem in general cannot be solved analytically. Thus, an artificial boundary condition imposed on the coarse grid boundary is needed to obtain a unique solution to the local cell problem. Among many choices of artificial boundary conditions, the uniform flux condition is a good choice, which is also successfully used for finding local basis functions for a multiscale flow problem in [18]. Therefore, we will numerically solve our local cell problem by imposing a Neumann boundary condition. In particular, we assume that the basis functions have unit flux on part of the cell boundary and zero flux on the rest of the boundary.

Now we will give a detail description of our new method. Assume Ω be the unit square $[0,1]^2$ which is uniformly triangulated by a set of squares $\mathcal{T}^H$ with side length $H>0$. The set $\mathcal{T}^H$ is our coarse mesh. A generic coarse grid block K in $\mathcal{T}^H$ with four boundary edges σ_E,σ_S,σ_W and σ_N is shown in Figure 1.

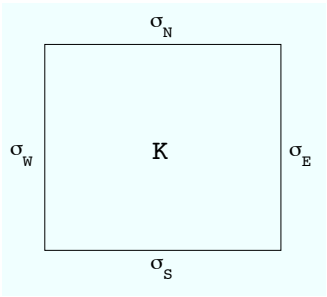

Figure 1: A generic coarse grid block.

For each $K\in\mathcal{T}^H$, we define the local basis functions w_1^K and w_2^K by

$$\begin{aligned} \mathcal{L}(w_i^K) &= 0, \qquad \text{in } K, \\ (\vec{b}w_i^K - a\nabla w_i^K)\cdot\vec{n} &= g_i, \qquad \text{on } \partial K, \end{aligned} \tag{2.1}$$

with the zero average condition $\int_K w_i^K\,dx=0$ where $\vec{n}$ denotes the outward unit normal vector on ∂K. In the above problem, the boundary functions g_i are defined by

$$\begin{aligned} g_1 &= 1 \quad \text{on } \sigma_E,\sigma_W \quad \text{and} \quad g_1 = 0 \quad \text{on } \sigma_N,\sigma_S, \\ g_2 &= 0 \quad \text{on } \sigma_E,\sigma_W \quad \text{and} \quad g_2 = 1 \quad \text{on } \sigma_N,\sigma_S. \end{aligned}$$

We remark that the above boundary conditions are the uniform flux conditions and are proved to be able to successfully capture the sub-grid behavior of a multiscale flow problem in [18]. Moreover, the functions w_1^K and w_2^K are solutions to the given differential operator $\mathcal{L}$ on a local cell K. It is well-known [13,17] that these functions provide important sub-grid features.

We will present the lowest order version of our method. Our finite element space $V(g)$ is defined by

$$V(g)=\{u\,|\,u|_K=\bar{u}^K+c_1^K w_1^K+c_2^K w_2^K\}.$$

We emphasize that the space $V(g)$ depends on the boundary function g specified in the boundary conditions in (1.1) and (1.2). The way that we impose this boundary condition in the space $V(g)$ will be discussed in the following paragraphs. Since the functions w_1^K and w_2^K have zero average, our solution space contains functions such that their restriction on each $K\in\mathcal{T}^H$ can be represented by cell average plus a linear combination of the functions w_1^K and w_2^K. We remark that similar function space has been used in [19] but the local basis functions w_1^K and w_2^K are obtained by solving the partial differential equation on a coarse grid analytically. With a complex media, this is relatively hard to do. Thus, we can see that our method is a kind of generalization of the successful method developed in [19] to problems with more complex media.

To define our new sub-grid enhanced IPDG method, we need the notion of jump and average of a function u in $H^1(K)$. Let $\mathcal{E}^H$ be the set of all edges in the triangulation $\mathcal{E}^H$. For each edge $\sigma\in\mathcal{E}^H$, we define a unit normal vector $\vec{n}_\sigma$ on σ which is pointing to the positive axis direction. Let σ be an edge and let K_1,K_2 be the corresponding cells which have this common edge. If the normal vector $\vec{n}_\sigma$ is pointing from K_1 to K_2, then we define the jump and the average of u on σ by

$$[u]_\sigma = u|_{K_1} - u|_{K_2} \quad \text{and} \quad \{u\}_\sigma = \frac{1}{2}(u|_{K_1} + u|_{K_2}).$$

If σ is a boundary edge, then one of the two values $u|_{K_1}$ and $u|_{K_2}$ have to be defined by using the boundary condition. This is discussed in the following paragraph.

Using the above definitions of jump and average of a function, we define the following bilinear form

$$\begin{aligned} B_H(u,v) &= \sum_{K\in\mathcal{T}^H}\Big(-\int_K(\vec{b}u - a\nabla u)\cdot\nabla v\Big) \\ &\quad + \sum_{\sigma\in\mathcal{E}^H}\Big(\int_\sigma(\vec{b}\cdot\vec{n}_\sigma\{u\}_\sigma - a\{\nabla u\cdot\vec{n}_\sigma\}_\sigma)[v]_\sigma + \int_\sigma a\{\nabla v\cdot\vec{n}_\sigma\}_\sigma[u]_\sigma + \frac{1}{2\delta}\int_\sigma a[u]_\sigma[v]_\sigma\Big) \end{aligned}$$

where $\delta>0$ is a penalty parameter to be specified. Then our new method for the approximation of (1.1) is formulated as follows: find $u_H\in V(g)$ such that

$$B_H(u_H,v) = \int_\Omega fv \quad \forall v\in V(0). \tag{2.2}$$

Note that this is the non-symmetric IPDG method [22]. The bilinear form B_h involves the jumps $[u]_\sigma$ and $[v]_\sigma$ that require the values of the functions u,v that are outside the domain Ω. For these values, we use the boundary condition specified in the spaces $V(g)$ and $V(0)$. In particular, for an boundary edge $\sigma\in\mathcal{E}^H$ with $\sigma\in\partial K$, we have $[u]_\sigma = g - u|_K$ where we assume that the unit normal vector on σ is pointing from outside of K to the inside of K. In the same way, we have $[v]_\sigma = 0 - v|_K$. The definition of $\{u\}_\sigma$ for a boundary edge σ is defined similarly by $\{u\}_e = \frac{1}{2}(g+u|_K)$. Moreover, B_h involves the averages $\{\nabla u\cdot\vec{n}_\sigma\}_\sigma$ and $\{\nabla v\cdot\vec{n}_\sigma\}_\sigma$ that require values of the fluxes outside the domain Ω. For these values, there

is no boundary condition that we can use. Nevertheless, if the given partial differential equation is solved on a larger domain that contains the given domain Ω, it is well-known that the flux of the solution on the set $\partial\Omega$ is continuous. This motivates us to assume that, for a boundary edge σ, the limiting value of the flux from outside the domain is equal to the limiting value of the flux from inside the domain. Thus, we define the quantities $\{\nabla u\cdot\vec{n}_\sigma\}_\sigma$ and $\{\nabla v\cdot\vec{n}_\sigma\}_\sigma$ by $\nabla u\cdot\vec{n}_\sigma$ and $\nabla v\cdot\vec{n}_\sigma$ respectively for a boundary edge σ.

For the time-dependent problem (1.2), we will use the transversal method of line approach. In particular, we apply the Crank-Nicolson method for the time discretization and obtain

$$\frac{u^{n+1}-u^n}{\Delta t}+\mathcal{L}\Big(\frac{1}{2}(u^{n+1}+u^n)\Big)=f^{n+\frac{1}{2}}$$

where $\Delta t>0$ is the time step size, $u^n=u(t_n,\cdot)$ and $t_n=n\Delta t$, $n=0,1,2,\cdots$. Thus, for each time step, we need to solve

$$\frac{2}{\Delta t}u+\mathcal{L}(u)=2f^{n+\frac{1}{2}}+\frac{2}{\Delta t}u^n-\mathcal{L}(u^n).$$

Our new DG space $V(g)$ provides an efficient way to solve this problem. In particular, given u^n, we need to find $u_H:=u^{n+1}\in V(g)$ by solving

$$\frac{2}{\Delta t}\int_\Omega u_Hv+B_H(u_H,v)=2\int_\Omega f^{n+\frac{1}{2}}v+\frac{2}{\Delta t}\int_\Omega u^nv-B_H(u^n,v),\quad\forall v\in V(0).$$

Another advantage of our method is that since a coarse mesh with mesh size $H>0$ is used, the time step size can also be chosen in the order of H, that is, $\Delta t=O(H)$. Hence, the time-marching is very efficient.

2.2 Stability

In this section, we will show that the discrete problem (2.2) is stable, and hence it is uniquely solvable. For any function $v\in V(0)$, we define the DG norm by

$$||v||_{DG}^2=\sum_{K\in\mathcal{T}^H}\int_K a|\nabla v|^2+\frac{1}{2\delta}\sum_{\sigma\in\mathcal{E}^H}\int_\sigma a[v]_\sigma^2.$$

Moreover, the problem (2.2) can be reformulated as: find $u_H\in V(0)$ such that

$$B_H(u_H,v)=\int_\Omega fv-\int_{\partial\Omega}\Big(\frac{\vec{b}\cdot\vec{n}_{\partial\Omega}}{2}g[v]-ag(\nabla v\cdot\vec{n}_{\partial\Omega})-\frac{1}{2\delta}ag[v]\Big),\quad\forall v\in V(0)\tag{2.3}$$

where the jump $[v]$ on the boundary of the domain $\partial\Omega$ is defined with respect to the unit outward normal vector $\vec{n}_{\partial\Omega}$ on $\partial\Omega$. First, we will prove the following coercivity condition for the bilinear form B_H.

Lemma 1. *For any $v\in V(0)$, we have $B_H(v,v)=||v||_{DG}^2$.*

Proof. Let $v \in V(0)$. Taking $u = v$ in the definition of B_H, we have

$$B_H(v,v) = \sum_{K\in\mathcal{T}^H} \Big(-\int_K (\vec{b}v - a\nabla v)\cdot\nabla v \Big) + \sum_{\sigma\in\mathcal{E}^H} \Big(\int_\sigma (\vec{b}\cdot\vec{n}_\sigma \{v\}_\sigma)[v]_\sigma + \frac{1}{2\delta}\int_\sigma a[v]_\sigma^2 \Big).$$

By using the definition of the DG norm, we obtain

$$B_H(v,v) = \|v\|_{DG}^2 + \sum_{K\in\mathcal{T}^H} \Big(-\int_K (\vec{b}v)\cdot\nabla v \Big) + \sum_{\sigma\in\mathcal{E}^H} \Big(\int_\sigma (\vec{b}\cdot\vec{n}_\sigma \{v\}_\sigma)[v]_\sigma \Big).$$

Therefore, it is sufficient to prove that

$$\sum_{K\in\mathcal{T}^H} \Big(-\int_K (\vec{b}v)\cdot\nabla v \Big) + \sum_{\sigma\in\mathcal{E}^H} \Big(\int_\sigma (\vec{b}\cdot\vec{n}_\sigma \{v\}_\sigma)[v]_\sigma \Big) = 0. \tag{2.4}$$

Since $\vec{b}$ is divergence free, for each $K \in \mathcal{T}^H$, we have

$$\begin{aligned}
\int_K (\vec{b}v)\cdot\nabla v &= \frac{1}{2}\int_K (\vec{b}v)\cdot\nabla v + \frac{1}{2}\int_K (\vec{b}v)\cdot\nabla v \\
&= \frac{1}{2}\int_K (\vec{b}v)\cdot\nabla v + \frac{1}{2}\Big(-\int_K \nabla\cdot(\vec{b}v)v + \int_{\partial K} (\vec{b}\cdot\vec{n}_{\partial K})v^2 \Big) \\
&= \frac{1}{2}\int_K (\vec{b}v)\cdot\nabla v - \frac{1}{2}\Big(\int_K (\nabla\cdot\vec{b})v^2 + \int_K (\vec{b}v)\cdot\nabla v \Big) + \frac{1}{2}\int_{\partial K} (\vec{b}\cdot\vec{n}_{\partial K})v^2 \\
&= \frac{1}{2}\int_{\partial K} (\vec{b}\cdot\vec{n}_{\partial K})v^2
\end{aligned}$$

where $\vec{n}_{\partial K}$ is the unit outward normal vector on ∂K. Moreover, we notice that, for each interior edge $\sigma \in \mathcal{E}^H$, we have

$$\int_\sigma (\vec{b}\cdot\vec{n}_\sigma \{v\}_\sigma)[v]_\sigma = \int_\sigma \frac{\vec{b}\cdot\vec{n}_\sigma}{2}(v^2|_{K_1} - v^2|_{K_2})$$

where $\vec{n}_\sigma$ is pointing from K_1 to K_2, and K_1,K_2 are two coarse grid blocks sharing the edge σ. Thus, we have

$$\int_\sigma (\vec{b}\cdot\vec{n}_\sigma \{v\}_\sigma)[v]_\sigma = \int_{\sigma\cap\partial K_1} \frac{\vec{b}\cdot\vec{n}_{\partial K_1}}{2} v^2|_{K_1} + \int_{\sigma\cap\partial K_2} \frac{\vec{b}\cdot\vec{n}_{\partial K_2}}{2} v^2|_{K_2}$$

where $\vec{n}_{\partial K_j}$ denotes the outward unit normal vector defined on ∂K_j with respect to K_j, for $j = 1,2$. For a boundary edge $\sigma \in \mathcal{E}^H$, since $v \in V(0)$, we have

$$\int_\sigma (\vec{b}\cdot\vec{n}_\sigma \{v\}_\sigma)[v]_\sigma = \int_{\sigma\cap\partial K} \frac{\vec{b}\cdot\vec{n}_{\partial K}}{2} v^2$$

where K is the coarse grid block with $\sigma \subset \partial K$. Consequently, we have

$$\sum_{\sigma\in\mathcal{E}^H}\int_\sigma(\vec{b}\cdot\vec{n}_\sigma\{v\}_\sigma)[v]_\sigma=\sum_{K\in\mathcal{T}^H}\int_{\partial K}\frac{\vec{b}\cdot\vec{n}_{\partial K}}{2}v^2=\sum_{K\in\mathcal{T}^H}\Big(\int_K(\vec{b}v)\cdot\nabla v\Big).$$

Therefore (2.4) holds. □

Next, we will estimate the right hand side of (2.3). Let $v\in V(0)$. First, we recall, from for example [3, 22], that the following discrete Poincare inequality

$$\|v\|^2_{L^2(\Omega)}\leq C_p\Big(\sum_{K\in\mathcal{T}^H}||\nabla v||^2_{L^2(K)}+\sum_{\sigma\in\mathcal{E}^H}\frac{1}{|\sigma|}||[v]_\sigma||^2_{L^2(\sigma)}\Big) \tag{2.5}$$

holds. Furthermore, the following Poincare inequality

$$\|v\|^2_{L^2(K)}\leq CH^2||\nabla v||^2_{L^2(K)} \tag{2.6}$$

holds when v has zero average in K, and the trace inequality

$$\|v\|^2_{L^2(\partial K)}\leq C\Big(H||\nabla v||^2_{L^2(K)}+\frac{1}{H}||v||^2_{L^2(K)}\Big) \tag{2.7}$$

holds. These inequalities will help us to estimate the right hand side of (2.3). The next lemma shows that the right hand side of (2.3) defines a continuous linear functional.

Lemma 2. *Assume that $\delta\leq\frac{H}{2}$. For all $v\in V(0)$, we have*

$$\left|\int_\Omega fv-\int_{\partial\Omega}\Big(\frac{\vec{b}\cdot\vec{n}_{\partial\Omega}}{2}g[v]-ag(\nabla v\cdot\vec{n}_{\partial\Omega})-\frac{1}{2\delta}ag[v]\Big)\right|\leq C||v||_{DG}\Big(\|f\|_{L^2(\Omega)}+\delta^{-\frac{1}{2}}\|g\|_{L^2(\partial\Omega)}\Big)$$

where the constant C is independent of the coarse mesh size H.

Proof. Let $v\in V(0)$. Then we decompose v into two parts and write $v=\bar{v}+\tilde{v}$ where $\bar{v}$ is the piecewise constant part of v and $\tilde{v}$ is the sub-grid enhanced part of v. More precisely, for each coarse grid block K, we can write

$$v|_K=\bar{v}|_K+\tilde{v}|_K$$

where $\bar{v}|_K$ is the average value of $v|_K$ on K and $\tilde{v}|_K=c_1^Kw_1^K+c_2^Kw_2^K$ for some coefficients c_1^K and c_2^K. It is easy to see that $\bar{v}$ and $\tilde{v}$ are $L^2(\Omega)$-orthogonal, that is,

$$\int_\Omega\bar{v}\tilde{v}=\sum_{K\in\mathcal{T}^H}\int_K\bar{v}|_K\tilde{v}|_K=0$$

since the basis functions w_1^K and w_2^K have zero average in the coarse grid block $K \in \mathcal{T}^H$. Then, using this decomposition of v, we can decompose the right hand side of (2.3) into five parts, namely,

$$\begin{aligned}
& \int_\Omega fv - \int_{\partial\Omega} \Big(\frac{\vec{b}\cdot\vec{n}_{\partial\Omega}}{2} g[v] - ag(\nabla v \cdot \vec{n}_{\partial\Omega}) - \frac{1}{2\delta} ag[v] \Big) \\
= & \int_\Omega fv - \int_{\partial\Omega} \Big(\frac{\vec{b}\cdot\vec{n}_{\partial\Omega}}{2} g[\bar{v}+\tilde{v}] - ag(\nabla \tilde{v} \cdot \vec{n}_{\partial\Omega}) - \frac{1}{2\delta} ag[v] \Big) \\
= & \int_\Omega fv - \int_{\partial\Omega} \Big(\frac{\vec{b}\cdot\vec{n}_{\partial\Omega}}{2} g[\bar{v}] - \frac{\vec{b}\cdot\vec{n}_{\partial\Omega}}{2} g[\tilde{v}] + \vec{b}\cdot\vec{n}_{\partial\Omega} g[\tilde{v}] - ag(\nabla \tilde{v} \cdot \vec{n}_{\partial\Omega}) - \frac{1}{2\delta} ag[v] \Big) \\
= & I_1 - I_2 + I_3 - I_4 + I_5
\end{aligned}$$

where

$$\begin{aligned}
I_1 &= \int_\Omega fv, \\
I_2 &= \int_{\partial\Omega} \frac{\vec{b}\cdot\vec{n}_{\partial\Omega}}{2} g[\bar{v}], \\
I_3 &= \int_{\partial\Omega} \frac{\vec{b}\cdot\vec{n}_{\partial\Omega}}{2} g[\tilde{v}], \\
I_4 &= \int_{\partial\Omega} \Big(\vec{b}\cdot\vec{n}_{\partial\Omega} g[\tilde{v}] - ag(\nabla \tilde{v} \cdot \vec{n}_{\partial\Omega}) \Big), \\
I_5 &= \frac{1}{2\delta} \int_{\partial\Omega} ag[v].
\end{aligned}$$

The terms I_1 and I_5 can be easily estimated by the Cauchy-Schwarz inequality, the definition of DG norm and (2.5). More precisely,

$$|I_1| \leq ||f||_{L^2(\Omega)} ||v||_{L^2(\Omega)} \leq C ||f||_{L^2(\Omega)} ||v||_{DG}.$$

Moreover, since a is bounded, we have

$$\begin{aligned}
|I_5| &= \frac{1}{2\delta} \int_{\partial\Omega} ag[v] \\
&\leq (2\delta)^{-\frac{1}{2}} ||a^{\frac{1}{2}} g||_{L^2(\partial\Omega)} \Big(\frac{1}{2\delta} \int_{\partial\Omega} a[v]^2 \Big)^{\frac{1}{2}} \\
&\leq C\delta^{-\frac{1}{2}} ||g||_{L^2(\partial\Omega)} ||v||_{DG}.
\end{aligned}$$

Next, we will estimate I_2 and I_3. We define $\mathcal{T}_1^H$ as the subset of $\mathcal{T}^H$ that contains all coarse grid blocks K with the property that at least one edge of K belongs to the boundary $\partial\Omega$. To estimate I_2, we use the fact that $\vec{b}$ is bounded and the Cauchy-Schwarz inequality

to obtain

$$|I_2| \leq CH^{-\frac{1}{2}}||g||_{L^2(\partial\Omega)} \left(\sum_{K\in\mathcal{T}_1^H} \left\| H^{\frac{1}{2}}\bar{v} \right\|^2_{L^2(\partial K\cap\partial\Omega)} \right)^{\frac{1}{2}}$$
$$\leq CH^{-\frac{1}{2}}||g||_{L^2(\partial\Omega)} \left(\sum_{K\in\mathcal{T}_1^H} \left\| H^{\frac{1}{2}}\bar{v} \right\|^2_{L^2(\partial K)} \right)^{\frac{1}{2}}.$$

Then the trace inequality (2.7) and the assumption $\delta < H/2$ imply

$$|I_2| \leq C\delta^{-\frac{1}{2}}||g||_{L^2(\partial\Omega)} \left(\sum_{K\in\mathcal{T}_1^H} \|\bar{v}\|^2_{L^2(K)} \right)^{\frac{1}{2}} \leq C\delta^{-\frac{1}{2}}||g||_{L^2(\partial\Omega)} \left(\sum_{K\in\mathcal{T}^H} \|\bar{v}\|^2_{L^2(K)} \right)^{\frac{1}{2}}.$$

By the fact that $\bar{v}$ and $\tilde{v}$ are $L^2(K)$-orthogonal,

$$|I_2| \leq C\delta^{-\frac{1}{2}}||g||_{L^2(\partial\Omega)} \left(\sum_{K\in\mathcal{T}^H} (\|\bar{v}\|^2_{L^2(K)} + \|\tilde{v}\|^2_{L^2(K)}) \right)^{\frac{1}{2}}$$
$$\leq C\delta^{-\frac{1}{2}}||g||_{L^2(\partial\Omega)} \left(\sum_{K\in\mathcal{T}^H} \|\bar{v}+\tilde{v}\|^2_{L^2(K)} \right)^{\frac{1}{2}}.$$

Thus, (2.5) yields

$$|I_2| \leq C\delta^{-\frac{1}{2}}||g||_{L^2(\partial\Omega)}||v||_{DG}.$$

To estimate I_3, we use a similar argument as above. First, by the assumption that $c_0 \leq a$, we have $\sum_{K\in\mathcal{T}^H} \|\nabla v\|^2_{L^2(K)} \leq \frac{1}{c_0}||v||^2_{DG}$. Then by the Cauchy-Schwarz inequality, we have

$$|I_3| \leq CH^{-\frac{1}{2}}||g||_{L^2(\partial\Omega)} \left(\sum_{K\in\mathcal{T}_1^H} \left\| H^{\frac{1}{2}}\tilde{v} \right\|^2_{L^2(\partial K\cap\partial\Omega)} \right)^{\frac{1}{2}}$$
$$\leq CH^{-\frac{1}{2}}||g||_{L^2(\partial\Omega)} \left(\sum_{K\in\mathcal{T}_1^H} \left\| H^{\frac{1}{2}}\tilde{v} \right\|^2_{L^2(\partial K)} \right)^{\frac{1}{2}}.$$

Using the trace inequality (2.7),

$$|I_3| \leq CH^{-\frac{1}{2}}||g||_{L^2(\partial\Omega)} \left(\sum_{K\in\mathcal{T}^H} (\|\tilde{v}\|^2_{L^2(K)} + H^2\|\nabla\tilde{v}\|^2_{L^2(K)}) \right)^{\frac{1}{2}}.$$

Since $\tilde{v}$ has zero average on each coarse grid block K, (2.6) yields

$$|I_3| \leq CH^{-\frac{1}{2}}||g||_{L^2(\partial\Omega)}\left(\sum_{K\in\mathcal{T}^H} H^2\|\nabla\tilde{v}\|^2_{L^2(K)}\right)^{\frac{1}{2}}.$$

Thus, we have

$$|I_3| \leq CH^{\frac{1}{2}}||g||_{L^2(\partial\Omega)}\left(\sum_{K\in\mathcal{T}^H} \|\nabla v\|^2_{L^2(K)}\right)^{\frac{1}{2}} \leq CH\delta^{-\frac{1}{2}}||g||_{L^2(\partial\Omega)}||v||_{DG}.$$

Finally we will estimate I_4. We first emphasize that, by definition, $\vec{b}\cdot\vec{n}_{\partial\Omega}\tilde{v} - a\nabla\tilde{v}\cdot\vec{n}_{\partial\Omega}$ is a constant on each $e\in\mathcal{E}^H$ with $e\subset\partial\Omega$. Let $e\subset\partial\Omega$ be a boundary edge. We define a quadratic polynomial w_e on e so that w_e equals zero at the two end points of e and equals $6(\vec{b}\cdot\vec{n}_{\partial\Omega}\tilde{v} - a\nabla\tilde{v}\cdot\vec{n}_{\partial\Omega})/4$ at the mid-point of e. Let K be the coarse grid block that has the edge e. Without loss of generality, we assume $\vec{n}_e = \vec{n}_{\partial\Omega}$. We can then define ϕ^e as the weak solution of the following problem

$$\begin{aligned} -\Delta\phi^e &= 0, \quad \text{in } K,\\ \phi^e &= w_e, \quad \text{on } e,\\ \phi^e &= 0, \quad \text{on } \partial K\backslash e. \end{aligned}$$

By standard theory, we have

$$\|\phi^e\|_{H^1(K)} \leq CH^{-\frac{1}{2}}\|w_e\|_{L^2(e)} \leq CH^{-\frac{1}{2}}||\vec{b}\cdot\vec{n}_e\tilde{v} - a\nabla\tilde{v}\cdot\vec{n}_e||_{L^2(e)}. \tag{2.8}$$

where the dependence on $H^{-\frac{1}{2}}$ is obtained by scaling argument. Since the basis functions are obtained by solving (2.1), we have

$$\int_K(\vec{b}\tilde{v} - a\nabla\tilde{v})\nabla\phi^e = \int_{\partial K}(\vec{b}\cdot\vec{n}_e\tilde{v} - a\nabla\tilde{v}\cdot\vec{n}_e)\phi^e.$$

By the boundary condition of ϕ^e defined above, we have

$$\int_K(\vec{b}\tilde{v} - a\nabla\tilde{v})\nabla\phi^e = \int_e(\vec{b}\cdot\vec{n}_e\tilde{v} - a\nabla\tilde{v}\cdot\vec{n}_e)\phi^e.$$

Using the Simpson's rule on the right hand side, we have

$$\int_K(\vec{b}\tilde{v} - a\nabla\tilde{v})\nabla\phi^e = H(\vec{b}\cdot\vec{n}_e\tilde{v} - a\nabla\tilde{v}\cdot\vec{n}_e)^2 = ||\vec{b}\cdot\vec{n}_e\tilde{v} - a\nabla\tilde{v}\cdot\vec{n}_e||^2_{L^2(e)}.$$

Thus,

$$||\vec{b}\cdot\vec{n}_e\tilde{v} - a\nabla\tilde{v}\cdot\vec{n}_e||^2_{L^2(e)} \leq C\Big(\|\tilde{v}\|_{L^2(K)} + \|\nabla\tilde{v}\|_{L^2(K)}\Big)\|\nabla\phi^e\|_{L^2(K)}$$

and (2.8) implies

$$||\vec{b}\cdot\vec{n}_e\tilde{v}-a\nabla\tilde{v}\cdot\vec{n}_e||_{L^2(e)}\leq CH^{-\frac{1}{2}}\Big(\|\tilde{v}\|_{L^2(K)}+\|\nabla\tilde{v}\|_{L^2(K)}\Big).$$

Hence, we obtain

$$\begin{aligned}|I_4|^2&\leq\|g\|^2_{L^2(\partial\Omega)}\|\vec{b}\cdot\vec{n}_e\tilde{v}-a\nabla\tilde{v}\cdot\vec{n}_e\|^2_{L^2(\partial\Omega)}\\&\leq CH^{-1}\|g\|^2_{L^2(\partial\Omega)}\sum_{K\in\mathcal{T}^H}\Big(\|\tilde{v}\|^2_{L^2(K)}+\|\nabla\tilde{v}\|^2_{L^2(K)}\Big)\\&\leq CH^{-1}\|g\|^2_{L^2(\partial\Omega)}\|v\|^2_{DG}.\end{aligned}$$

Combining all results above, we obtain the required estimate. □

Finally, we state and prove our main result of this section.

Theorem 3. *Let $u_H\in V(0)$ be the solution of (2.3) and $\delta\leq H/2$. Then, for $H\leq H_0$, we have*

$$\|u_H\|_{DG}\leq C\Big(\|f\|_{L^2(\Omega)}+\delta^{-\frac{1}{2}}\|g\|_{L^2(\partial\Omega)}\Big).$$

Proof. By the above two lemmas,

$$\begin{aligned}\|u_H\|^2_{DG}&=B_H(u_H,u_H)\\&=\int_\Omega fu_H-\int_{\partial\Omega}\Big(\frac{\vec{b}\cdot\vec{n}_{\partial\Omega}}{2}g[u_H]-ag(\nabla u_H\cdot\vec{n}_{\partial\Omega})-\frac{1}{2\delta}ag[u_H]\Big)\\&\leq C||u_H||_{DG}\Big(\|f\|_{L^2(\Omega)}+\delta^{-\frac{1}{2}}\|g\|_{L^2(\partial\Omega)}\Big),\end{aligned}$$

and the theorem is proved. □

We remark that the factor of $\delta^{-\frac{1}{2}}$ in the above estimate is common for IPDG method, see [22]. This is because the Dirichlet boundary condition is imposed weakly in (2.3).

3 Numerical Results

In this section, we will present some numerical examples to illustrate the accuracy of our new IPDG approach. We use $H>0$ to represent the coarse mesh size and $h>0$ to represent fine mesh size which is used to compute the reference solutions and to numerically solve the local basis functions w_i^K. We also use u,u_h,u_c and u_b to represent the exact/reference solution, numerical solution obtained by our sub-grid structure enhanced IPDG method, numerical solution obtained by classical central difference method and numerical solution obtained by classical upwind difference method respectively. In the following sections, we will compute and compare the following error quantities

$$E=\frac{\|u_h-u\|_2}{\|u\|_2},\quad E_c=\frac{\|u_c-u\|_2}{\|u\|_2}\quad\text{and}\quad E_b=\frac{\|u_b-u\|_2}{\|u\|_2}$$

where $\|\cdot\|_2$ denotes L^2 norm. Unless specified, the Dirichlet boundary data g is assumed to be zero.

3.1 Accuracy and convergence tests

We will test the accuracy and convergence rate of our method applied to the convection-diffusion problem (1.1) with a, $\vec{b}$ and f chosen as follows:

$$a=\frac{1.2+\sin(19\pi x)\cos(31\pi y)}{1.2+\sin(43\pi x)\sin(43\pi y)},\quad \vec{b}=\begin{pmatrix}\sin(2\pi x)\cos(2\pi y)\\ -\cos(2\pi x)\sin(2\pi y)\end{pmatrix}\quad\text{and}\quad f=1.$$

For these tests, the penalty parameter is chosen as $\delta=H/2$ and a reference solution is obtained with the mesh size $h=1/800$. First, we will consider the case with fixed fine mesh size ($h=1/800$) and test the convergence with different coarse mesh sizes $H=1/10$,$1/20$ and $1/40$. For these three cases, the local problems for finding basis functions on coarse grids are obtained with grid sizes 80×80, 40×40 and 20×20 respectively. The relative errors for numerical solutions computed by our method and the classical central difference method are shown in Table 1. We observe, from the second column of Table 1, that our method gives first order rate of convergence with respect to the coarse mesh size H. This result agrees with the fact that our DG finite element space $V(0)$ contains piecewise constant functions. Also, from the second and the third columns of Table 1, we see that our method produces more accurate solutions compared with the classical central difference method. In particular, with a very coarse mesh size $H=1/10$, our method produces a numerical solution with relative error of 7.34% while the central difference method gives a relative error of 18.3%. As the coarse mesh size is reduced to $H=1/40$, our method still performs better, giving a relative error of 1.5% while the central difference method gives a relative error of 3.34%. In addition, we see that the error difference between the two methods is decreased when smaller coarse mesh size is used. We expect that when very fine coarse mesh is used, the errors of the two methods should tend to identical.

Besides, we will perform accuracy and convergence rate tests with various coarse mesh sizes and a fixed local problem size. The coarse mesh sizes we used are $H=1/10$,$1/20$ and $1/40$ while the local problems for solving the basis functions are defined on a 20×20 grid. Thus, the fine mesh sizes, which are used to discretize the local problems, are $h=1/200$,$1/400$ and $1/800$ respectively. The relative errors for the numerical solutions obtained by our method for the above three settings are shown in Table 2. We see that the relative error is reduced approximately by a factor of two when the coarse mesh size is also reduced by a factor of two. This numerical result shows that our method has a first order convergence with respect to the coarse mesh size when the local problem size is fixed.

Furthermore, for a comparison, the reference solution, numerical solution computed by our method with coarse mesh size $H=1/20$ and the central difference solution with mesh size $H=1/20$ are shown in Figure 2. From the middle plot of Figure 2, we see

that our method is able to produce a numerical solution with the correct coarse behavior. On the contrary, the central difference method is unable to perform well. From the right plot of Figure 2, we see that the central difference solution contains some unwanted oscillations near the domain boundary, and does not give the correct coarse behavior.

H	E	E_c
1/10	0.0734	0.1830
1/20	0.0306	0.0924
1/40	0.0150	0.0334

Table 1: Relative errors for convection-diffusion problem with a fixed fine mesh size.

H	h	E
1/10	1/200	0.0826
1/20	1/400	0.0327
1/40	1/800	0.0150

Table 2: Relative errors for convection-diffusion problem with a fixed local problem size.

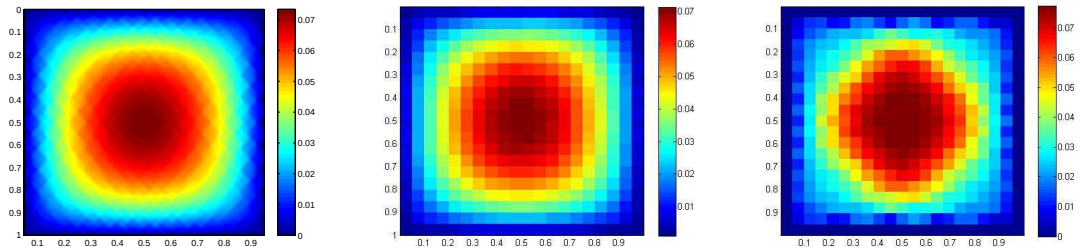

Figure 2: Left: Reference solution with mesh size $h=1/800$. Middle: Solution obtained by our method with mesh size $H=1/20$. Right: Solution obtained by central difference with mesh size $H=1/20$.

3.2 Performance with internal or boundary layers

In this section, we illustrate the performance of our new method for static convection-dominated diffusion problems with boundary or internal layers. First, we consider a problem with a boundary layer. We choose the following problem setting:

$$a=\frac{1}{100},\quad \vec{b}=\begin{pmatrix}1\\2\end{pmatrix}\quad \text{and}\quad f=1.$$

For the penalty parameter, we take $\delta=1/100$. A reference solution is again obtained with mesh size $h=1/800$. The numerical solutions using our method, the central difference

method and the upwind difference method are obtained with a coarse mesh size $H = 1/20$. The numerical results are shown in Figure 3. From the two figures on the top of Figure 3, we see that our method can accurately capture the coarse behavior of the solution. Moreover, the boundary layer of the solution is accurately computed, without artificial oscillations. Since we are using a coarse grid to approximate the solution, the boundary layer, as it can be seen in the top-right figure of Figure 3, is only captured on the coarse grid level, and this is the reason for the thick layer near the bottom part of the domain. From the bottom-left figure of Figure 3, however, we see that the central difference method produces a solution that is oscillating which is a well-known result. In the bottom-right figure of Figure 3, we compare the behavior of the 4 solutions on the line defined by $x = 0.925$, where we use red dash line and blue line to represent the solution obtained by our method and the reference solution respectively. We see that the upwind difference method (red solid line) produces a solution that is smeared too much and the central difference method (green line) produces an oscillatory solution. In terms of relative errors, we obtain a relative error of 12.38% for our method. For central and upwind difference methods, the relative errors are 23.02% and 22.50% respectively. We see that among the 3 numerical solutions, our method gives the most accurate result.

In Table 3, we present some numerical results to further analyze the accuracy of the numerical solutions computed by our method, and compare its performance with the central difference method and the upwind difference method for various coarse mesh sizes. From the table, we see that performance of our method is significantly better than that of the upwind difference method for the 3 coarse mesh sizes we used. Moreover, with coarse mesh sizes $H = 1/10$ and $H = 1/20$, our method shows better accuracy compared with the central difference method. For the case with coarse mesh sizes $H = 1/40$, the relative errors for our method and the central difference method are about the same. This is due to the fact that for this mesh size, the central difference method is able to eliminate the artificial oscillations.

H	E	E_c	E_b
1/10	0.1636	0.4653	0.3570
1/20	0.1238	0.2302	0.2250
1/40	0.0949	0.0960	0.1331

Table 3: Relative errors for a problem with a boundary layer.

Next we consider a problem with an internal layer. The coefficients and source data are chosen as follows:

$$a = \frac{1}{400} + \frac{\cos^2(22\pi x)\cos^2(38\pi y)}{2}, \quad \vec{b} = \begin{pmatrix} 1 \\ 2 \end{pmatrix} \quad \text{and} \quad f = 1.$$

We also take a non-homogeneous Dirichlet boundary condition for which the function g

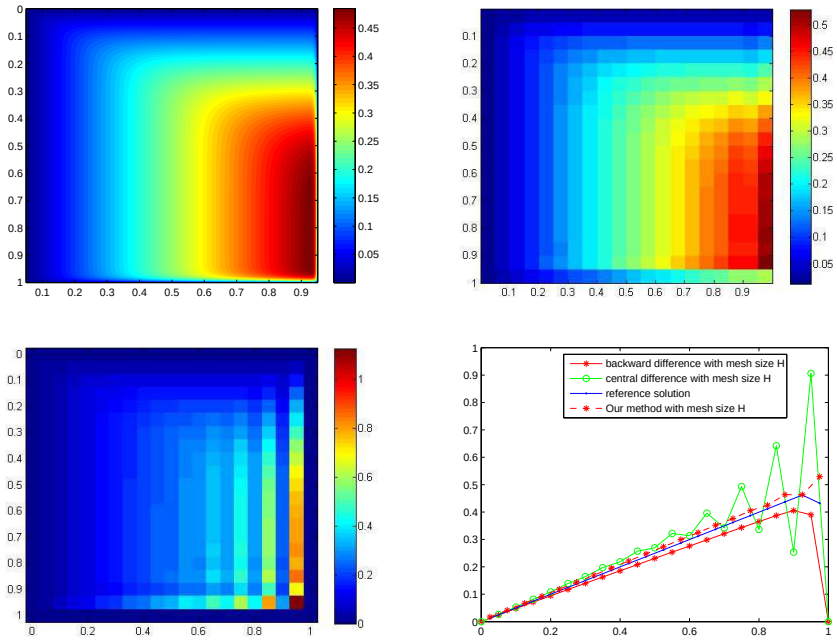

Figure 3: Top-left: Reference solution with mesh size $h=1/800$. Top-right: Solution obtained by our method with mesh size $H=1/20$. Bottom-left: Solution obtained by central difference with mesh size $H=1/20$. Bottom-right: Comparison of solutions on the line $x=0.925$.

is defined by

$$g=1 \quad \text{on} \quad \{0.25\leq x\leq 1,\ y=0\}\cup\{0.75\leq x\leq 1,\ y=1\}\cup\{x=0,\ 0\leq y\leq 1\}$$

and $g=0$ otherwise. The penalty parameter is chosen as $\delta=H/2$. For the comparison of accuracy, a reference solution is obtained with mesh size $h=1/800$ and is shown in Figure 4. Using the coarse mesh size $H=1/40$, three numerical solutions computed by our method, the central difference method and the upwind difference method are obtained, and the results are shown in Figure 4. From the two figures on the top of Figure 4, we see that our method is able to capture this internal layer accurately. Moreover, most structures of the solution are computed precisely. On the contrary, from the bottom-left figure of Figure 4, we see that the central difference method produces a solution that is oscillatory near the boundary $\{x=1\}$, and the internal layer of the exact solution is not captured. From the bottom-right figure of Figure 4 we see that the backward difference method produces a solution that is smeared out too much, as evident from the magnitude of the numerical solution. Also, the internal layer cannot be accurately computed. Regrading errors, the relative error is 5.27% for our method. For central and upwind difference methods, the relative errors are 12.26% and 11.28% respectively. We see that our method is significantly better than the classical methods.

In Table 4, we present some numerical results to further analyze the accuracy of the

numerical solutions computed by our method, and compare its performance with the central difference method and the upwind difference method for various coarse mesh sizes. From this table, we see that performance of our method is significantly better than that of the central and upwind difference methods for the 3 coarse mesh sizes we used. We also see that for the coarse mesh size $H = 1/10$, all the three methods are unable to perform well with the upwind difference method performs a bit better. With the refinement of the coarse mesh size, we see that the error for our method improves significantly while the errors for the other two methods improve only slightly. Consequently, we see that in order to obtain a reasonably accurate solution, we need the coarse mesh size to be fine enough but it is no need to be taken too small to resolve all details.

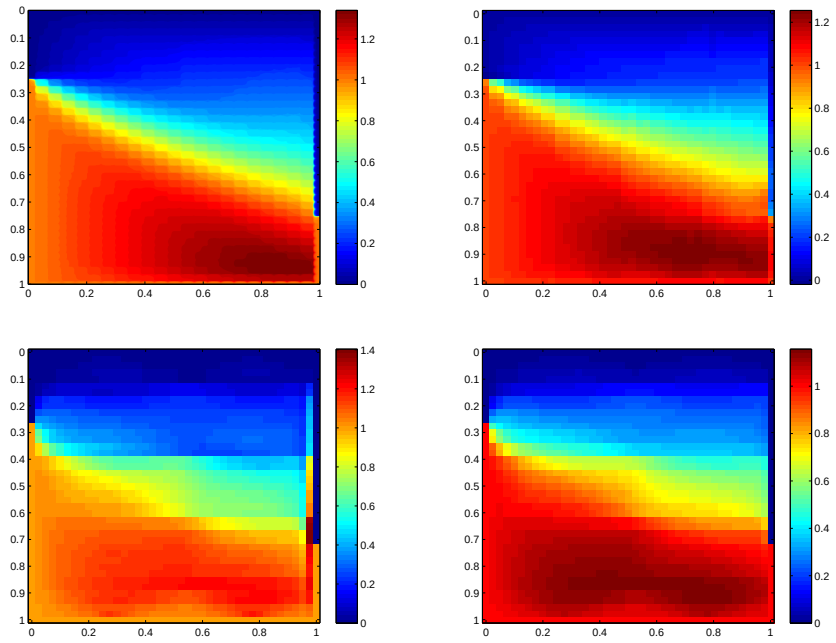

Figure 4: Top-left: Reference solution obtained with mesh size $h = 1/800$. Top-right: Solution obtained by our method with mesh size $H = 1/40$. Bottom-left: Solution obtained by central difference with mesh size $H = 1/40$. Bottom-right: Solution obtained by upwind difference with mesh size $H = 1/40$.

H	E	E_c	E_b
1/10	0.1703	0.1798	0.1511
1/20	0.0888	0.1373	0.1376
1/40	0.0527	0.1226	0.1128

Table 4: Relative errors for a problem with an internal layer.

3.3 Time-dependent problems

We now turn our discussion to time-dependent problems. We will consider a convection-diffusion problem in non-homogeneous media which is defined by the following settings:

$$a=\frac{1.2+\sin(11\pi x)\cos(11\pi y)}{1.2+\sin(43\pi x)\sin(43\pi y)},\quad \vec{b}=\begin{pmatrix}\sin(21\pi x)\cos(21\pi y)+2\\ -\cos(21\pi x)\sin(21\pi y)+2\end{pmatrix}\quad\text{and}\quad f=(t+0.2)^{-3}$$

with homogeneous initial condition $u_0=0$. The penalty parameter is taken as $\delta=H/2$ and a reference solution is computed on a fine grid with mesh size $h=1/800$. We will compare the accuracy of the solutions obtained by our method and the central difference method at various times and for various choices of coarse mesh sizes and time steps. The relative errors for these cases are shown in Tables 5-7. In Table 5, the relative errors for the solution obtained by our method at the time $T=0.3$ are shown on the left while the relative errors for the solution obtained by the central difference method at the same time $T=0.3$ are shown on the right. From the table on the left, we see the convergence of our method with respect to the coarse mesh size H. In particular, when the time step size is taken as $\Delta t=H$, the time step size is comparatively large and the time discretization error dominates. This is confirmed by the second order convergence of the errors in the third column of the left table of Table 5. On the other hand, when the time step size is taken as $\Delta t=H/4$, the time step size is comparatively small and the spatial discretization error dominates. This is again confirmed by the first order convergence of the errors in the fourth column of the left table in Table 5. On the contrary, from the right table of Table 5, we see that the accuracy of using standard central difference method is much lower than that of our method. For instance, when the coarse mesh size is $H=1/40$ and the time step size is $\Delta t=H/4$, the relative error of the solution computed by our method is approximately 1% while the relative error of the solution computed by the central difference method is about 17%. In Table 6 and Table 7, a similar comparison is performed when the solution is computed at the time $T=0.4$ and $T=0.5$ respectively, and a similar conclusion is obtained.

H	$\Delta t=H$	$\Delta t=H/2$	$\Delta t=H/4$
1/10	0.3895	0.0808	0.0418
1/20	0.0753	0.0212	0.0174
1/40	0.0184	0.0102	0.0095

H	$\Delta t=H$	$\Delta t=H/2$	$\Delta t=H/4$
1/10	0.4369	0.2725	0.2602
1/20	0.2405	0.2248	0.2218
1/40	0.1777	0.1728	0.1719

Table 5: Comparison of relative errors at time $T=0.3$. Left: our method. Right: central difference.

3.4 Performance with more general media

In this final section, we will illustrate the performance of our new IPDG method for convection-diffusion problems in more general media. First, we will consider a convection-

H	$\Delta t = H$	$\Delta t = H/2$	$\Delta t = H/4$
1/10	0.4991	0.0910	0.0431
1/20	0.0984	0.0226	0.0177
1/40	0.0219	0.0100	0.0094

H	$\Delta t = H$	$\Delta t = H/2$	$\Delta t = H/4$
1/10	0.3800	0.2564	0.2483
1/20	0.2279	0.2138	0.2117
1/40	0.1703	0.1660	0.1652

Table 6: Comparison of relative errors at time $T = 0.4$. Left: our method. Right: central difference.

H	$\Delta t = H$	$\Delta t = H/2$	$\Delta t = H/4$
1/10	0.6521	0.1008	0.0447
1/20	0.1266	0.0242	0.0179
1/40	0.0261	0.0098	0.0092

H	$\Delta t = H$	$\Delta t = H/2$	$\Delta t = H/4$
1/10	0.5089	0.2417	0.2369
1/20	0.2175	0.2031	0.2016
1/40	0.1628	0.1588	0.1582

Table 7: Comparison of relative errors at time $T = 0.5$. Left: our method. Right: central difference.

diffusion problem in a random medium, for which the coefficient a is taken as the function shown in the left plot in Figure 5.

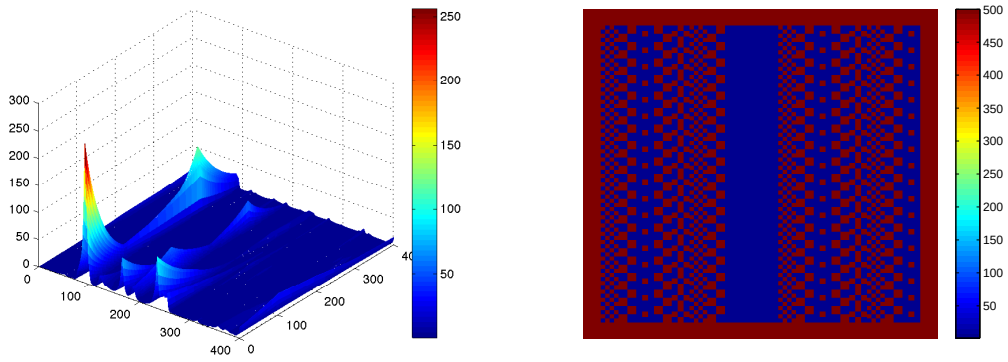

Figure 5: Left: A random medium. Right: A medium with checkerboard structure.

From Figure 5, we see that the medium has some random non-local features as well as large contrasts. It is also defined on a 400×400 grid. For the other parameters of the problem, we take

$$\vec{b} = \begin{pmatrix} 1 \\ 2 \end{pmatrix} \quad \text{and} \quad f = 2.$$

The penalty parameter is chosen as $\delta = H/2$. A reference solution is obtained with $h = 1/400$. The relative errors for various coarse mesh size are shown in Table 8. We see that the relative error for the solution computed by our method is reduced by a factor of two when the coarse mesh size is also reduced by a factor of two. However, the relative error for the solution computed by the central difference method does not decrease

much as coarse mesh size is decreased. Comparing the two schemes, we see that when the coarse mesh size is $H=1/10$, the relative errors for the solutions computed by our method and the central difference method are 11.23% and 97.08% respectively. When the coarse mesh size is reduced to $H=1/40$, the errors are 3.03% and 17.94% respectively. Therefore, it is evident that our method has a first order convergence rate and that the error for the solution computed by our method is much lower than that of the central difference approximation. Reference and numerical solutions computed by our method and the central difference method are shown in Figure 6. On the top row of Figure 6, we present the reference solution defined on the original 400×400 fine grid and the reference solution projected to the coarse grid with $H=1/20$. We note that the projected reference solution is for comparison purpose. In the bottom-left figure of Figure 6, the numerical solution computed by our method with $H=1/20$ is shown. Comparing this and the projected reference solution, we see that all features of the exact solution are captured by our scheme, and the relative error is only 6.41%. On the other hand, in the bottom-right figure of Figure 6, the numerical solution computed by the finite difference method, with a relative error of 18.58%, by the same coarse mesh is shown. It is clear that some features of the exact solution are missing.

H	E	E_c
1/10	0.1123	0.9708
1/20	0.0641	0.1858
1/40	0.0303	0.1794

Table 8: Relative errors with fixed fine mesh size.

Next we will consider a medium with a checker-board structure, shown in the right diagram of Figure 5. In this case, the diffusion coefficient $a(x)$ has a very high contrast, with the value 1 in the blue region and the value 500 in the red region. Thus, there are both convection-dominated and diffusion dominated regions. The vector $\vec{b}$, the function f and the boundary condition g are defined as follows:

$$\vec{b}=\begin{pmatrix} -100 \\ 100 \end{pmatrix}, \qquad f=0$$
$$g(x,y)=1 \quad x=1 \text{ or } y=0, \qquad g(x,y)=0 \quad \text{otherwise}.$$

A reference solution is obtained using the fine mesh size $h=1/960$ and the penalty parameter is chosen as $\delta=H/2$. We will illustrate the performance of our scheme with a coarse mesh size $H=1/40$. In Figure 7, the reference solution, the numerical solution computed by our method and the central difference method are shown. From the top two diagrams of Figure 7, we see that our method is able to capture the behavior of the exact solution. In particular, both the narrow layer near the boundary and the interior structures of the solution are accurately computed. As a comparison, we also show the

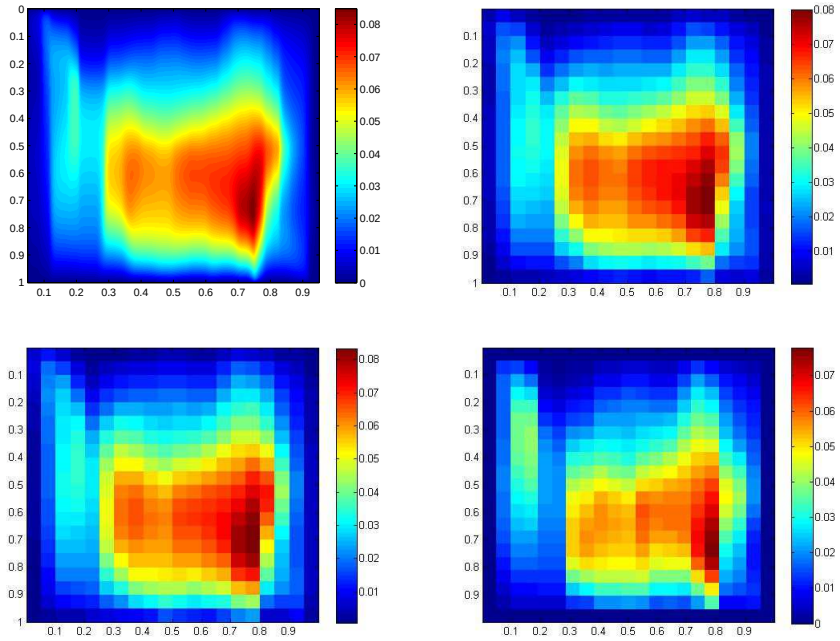

Figure 6: Top-left: Reference solution with mesh size $h = 1/400$. Top-right: Reference solution projected to a coarse mesh with $H = 1/20$. Bottom-left: Solution obtained by our method with mesh size $H = 1/20$. Bottom-right: Solution obtained by central difference with mesh size $H = 1/20$.

numerical solutions obtained by the classical central difference method. In the bottom left diagram of Figure 7, we present the case with the coefficient $a(x)$ is averaged out on each coarse grid while in the bottom right diagram of Figure 7, we present the case that the coefficient $a(x)$ is not averaged out. We see that in both cases, the finite difference method cannot produce an accurate numerical solution on a coarse grid with mesh size $H = 1/40$. Moreover, in terms of accuracy, the relative error is 5.23% for our method and it is 15.54% and 29.16% for finite difference with average and non-average coefficients respectively. Therefore, we see that our new IPDG method is able to produce an accurate numerical solution on a relatively coarse grid.

4 Conclusion

In this paper, we present and study a new sub-grid enhanced IPDG method for diffusion and convection-diffusion problems in heterogeneous media as well as convection-dominated problems. The formulation of the discrete problem is based on the IPDG approach, and the main contribution and success of this work is the choice of the local approximation space. The finite element space contains two components, one is the classical polynomial space and the other is spanned by local basis functions which are

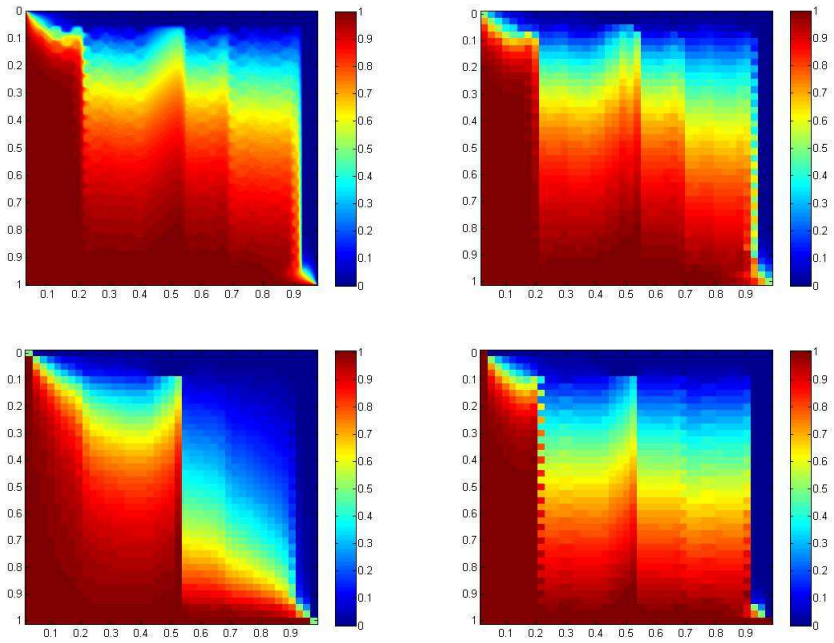

Figure 7: Top-left: Reference solution with mesh size $h=1/960$. Top-right: Solution obtained by our method with mesh size $H=1/40$. Bottom-left: Solution obtained by central difference with averaged coefficient and mesh size $H=1/40$. Bottom-right: Solution obtained by central difference with non-averaged coefficient and mesh size $H=1/40$.

solution of local cell problems. The key feature is that we do not assume that these local problems can be solve analytically, which allows our method to handle more complex media. Stability of our method is proved, and extensive numerical results show that our method is able to capture the coarse scale behavior of the exact solution on a coarse grid. In the future, we plan to further enhance the accuracy of our method by using higher order basis functions.

Acknowledgement

The authors would like to thank the reviewers' careful reading of the paper as well as their constructive comments and suggestions, which greatly enhance the paper. The work described in this paper was fully supported by a grant from the Research Grant Council of the Hong Kong SAR (Project no. CUHK401010).

References

[1] D. N. Arnold. *An interior penalty finite element method with discontinuous elements*. SIAM J. Numer. Anal., 19 (1982), pp. 742–760.

[2] D. N. Arnold, F. Brezzi, B. Cockburn and L. D. Marini. *Unified analysis of discontinuous Galerkin methods for elliptic problems*. SIAM J. Numer. Anal., 39 (2002), pp. 1749–1779.
[3] S. Brenner. *Poincaré-Friedrichs inequalities for piecewise H^1 functions*. SIAM J. Numer. Anal., 41 (2003), pp. 306–324.
[4] P. Castillo, B. Cockburn, I. Perugia and D. Schötzau. *An a priori error analysis of the local discontinuous Galerkin method for elliptic problems*. SIAM J. Numer. Anal., 38 (2000), pp. 1676–1706.
[5] E. Chung and Y. Efendiev. *Reduced contrast approximations for high-contrast multiscale flow problems*. SIAM MMS , 8 (2010), pp. 1126–1153.
[6] E. Chung, Y. Efendiev and R. Gibson. *An energy-conserving discontinuous multiscale finite element method for the wave equation in heterogeneous media*. Advances in Adaptive Data Analysis, 3 (2011), pp. 251–268.
[7] E. Chung and B. Engquist. *Optimal discontinuous galerkin methods for wave propagation*. SIAM J. Numer. Anal., 44 (2006), pp. 2131–2158.
[8] E. Chung and B. Engquist. *Optimal discontinuous Galerkin methods for the acoustic wave equation in higher dimensions*. SIAM J. Numer. Anal., 47 (2009), pp. 3820–3848.
[9] E. Chung and C. Lee. *A staggered discontinuous Galerkin method for the curl-curl operator*. To appear in IMA J. Numer. Anal.
[10] E. Chung and C. Lee. *A staggered discontinuous Galerkin method for the convection-diffusion equation*. J. Numer. Math., 20 (2012), pp. 1–31.
[11] B. Cockburn and C.-W. Shu. *The local discontinuous Galerkin method for time-dependent convection-diffusion systems*. SIAM J. Numer. Anal., 35 (1998), pp. 2440–2463.
[12] W. E and B. Engquist. *The heterogeneous multiscale methods*. Commun. Math. Sci., 1 (2003), pp. 87–132.
[13] Y. Efendiev and T. Y. Hou. *Multiscale finite element methods, volume 4 of Surveys and Tutorials in the Applied Mathematical Sciences*. Springer, New York, 2009.
[14] Y. Efendiev, T. Hou and X. Wu. *Convergence of a nonconformal multiscale finite element method*. SIAM J. Numer. Anal., 37 (2000), pp. 888–910.
[15] R. Gibson, K. Gao, E. Chung and Y. Efendiev. *Multiscale modeling of acoustic wave propagation in two-dimensional media*. Submitted.
[16] T. Y. Hou and D. Liang. *Multiscale analysis for convection dominated transport equations*. DCDS-A, 23 (2009), pp. 281–298.
[17] T. Hou and X. Wu. *A multiscale finite element method for elliptic problems in composite materials and porous media*. J. Comput. Phys., 134 (1997), pp. 169–189.
[18] P. Jenny, S.H. Lee and H.A. Tchelepi. *Multi-scale finite-volume method for elliptic problems in subsurface flow simulation* J. Comput. Phys., 187 (2003), pp. 47–67.
[19] I. Kalashnikova, C. Farhat and R. Tezaur. *A discontinuous enrichment method for the finite element solution of high Péclet advection-diffusion problems*. Finite elements in Analysis and Design, 45 (2009), pp. 238–250.
[20] H. Owhadi and L. Zhang. *Metric-based upscaling*. Comm. Pure Appl. Math., 60 (2007), pp. 675–723.
[21] P. Park and T. Y. Hou. *Multiscale numerical methods for singularly-perturbed convection diffusion equations*. International Journal of Computational Methods, 1 (2004), pp. 17–65.
[22] B. Rivière. *Discontinuous Galerkin methods for solving elliptic and parabolic equations*. SIAM, 2008.
[23] W. Wang, J. Guzman and C. Shu. *The multiscale discontinuous Galerkin method for solving a class of second order elliptic problems with rough coefficients*. Int. J. Numer. Anal. Model., 8 (2011), pp. 28–47.